USER FRIENDLY FINITE ELEMENT DESIGN OF SHAFTS AND TUNNELS

William G. Pariseau, Department of Mining Engineering, University of Utah
Mark K. Larson, Heather E. Lawson, CDC NIOSH, Spokane, WA

ABSTRACT

Rational design based on engineering fundamentals is essential for the layout of safe, stable shafts and tunnels. Shafts and tunnels including winzes, raises, adits, and crosscuts are lifelines to the underground and must be secure. The contribution of this paper describes a significant extension in existing software previously developed for five important design problems in strata-bound mines such as coal, trona, salt, potash, and some large, lead-zinc mines. This extension in software allows analysis to proceed in three easy steps: (1) preparation of a strata properties file, (2) generation of the finite element model, a mesh, and (3) finite element program execution. Circular, elliptical, and rectangular shaft sections are available for a single shaft, twin shafts, and shafts in a row. Spacing of twin shafts and shafts in a row is a free parameter (pillar width). Tunnel shapes are the same as shafts but include the conventional arched back section. Dipping strata of variable thickness, depth and orientation relative to the excavation of choice are allowed. The analyses are three-dimensional. An elastic-plastic material model based on associated rules of flow and an N-type yield condition for isotropic, transversely isotropic, or orthotropic rock are used for all strata. Example analyses from several hardrock mines are provided to illustrate the three-step process including mesh plotting and plotting of selected results. The goal of this software is to advance mine design technology for improved miner health and safety.

INTRODUCTION

This contribution describes an extension of previous work (Pariseau et al. 2017; Pariseau et al. 2020) from user-friendly finite element analysis of

(1) main entries,
(2) barrier pillars,
(3) bleeder entries,
(4) interpanel barrier pillars, and
(5) safety of rooms and pillars in room and pillar mining

to include

(6) shafts, winzes, raises, and
(7) tunnels, adits, and crosscuts.

In every case, the procedure is the same user friendly three-step process: (1) preparation of a strata properties file, (2) interactive mesh generation, and (3) program execution. The interactive mesh generator automates mesh generation for the seven problems mentioned with a short script of input prompts so that the user does not need to be an expert modeler to construct a good mesh. Such capability provides a powerful tool to mine engineers who have the most need for such design analysis Thus, “user-friendly” in this paper refers to .the relative confidence that mine engineers can use the tool compared to a FEA software having much more freedom to make poor choices in model construction.

PROBLEM STATEMENT

The design problem is addressed by first performing an analysis of stress, given the site stratigraphy, strata properties, in-situ stress, and proposed excavation shape and dimensions. An analysis of stress includes a computation of displacements, strains, and stresses induced by the proposed excavation. An elastic material model is reasonable in almost all cases of excavation in rock. However, the range of a purely elastic response to load is certainly limited by strata strength. Subsequent deformation may be strain softening, hardening, or neither. Elastic-ideally plastic is the choice to use in the finite element analysis software here. Directional properties associated with strata foliation may be present as well as in previously mined sections.

An important feature of any problem in rock mechanics design is jointing. Indeed, joints distinguish rock mechanics as a unique discipline in the mechanics of solids. Joints are almost always absent in laboratory-scale testing for rock properties (elastic moduli and strengths); usually joints appear at the meter scale in situ. How joints affect strata properties is often a matter of conjecture, although there are numerous jointed rock models described in the extensive technical literature (Beran 1968; Duncan and Goodman 1968; Salamon 1968; Morland 1974; Amadei and Goodman 1981; Gerrard 1982; Shi et al. 1985; Teply and Dvorak 1987; Pinto da Cunha 1990; Pariseau 1995). In this regard, elastic moduli computed from equilibrium and compatible models fall within lower and upper bounds given by theorems in solid mechanics (Hashin and Shtrikman 1963; Hill 1967; Huet 1984).

Almost all jointed rock models include the assumption of a representative volume element (RVE). An RVE contains many joints; one joint more or less has little effect on the moduli of the composite sample. The requirement of an RVE is a serious limitation.

An *optimum* jointed rock model in the elastic domain is one that satisfies the long-established criteria for stability at an interface. Hudson (1980) presents a succinct explanation of these criteria, attributed to Hadamard (1903), which are essentially continuity conditions for traction and displacement**.** This model allows for multiple joint sets (Pariseau 1988; Pariseau and Moon 1988). Moreover, the sample (element) size in this model need not be an RVE. This model feature is essential for numerical analysis where elements range from the small near an excavation wall to much larger elements away from the excavation.

Joints from a given joint set are embedded in the finite element mesh at hand one after the other according to joint dip, dip direction, and spacing. Each joint set is processed in turn; each joint set may have different properties. Accordingly, an element may be joint-free or may contain numerous joint segments associated with intersections of joints from different joint sets. Elements that contain joints are composite materials composed of joints and intact rock between joints and have equivalent elastic moduli that are unique; that is, each element may have different elastic moduli. In this regard, joint segments and intact rock have different strengths and may fail at different load levels during an analysis. While there are equivalent elastic moduli, there are no equivalent strengths. In any case, elastic-plastic behavior ensues whenever any joint segment in an element or the intact rock in an element reaches the elastic limit. The entire process is automatic and implemented much the same as an ordinary finite element analysis, as examples show in what follows.

PROBLEM APPROACH

The well-known finite element method of analysis provides an easy avenue to rational design by providing distributions of stress, strain, and displacement induced by a proposed shaft or tunnel layout. Of particular importance is the extent of yielding, if any, about the proposed excavation. While some yielding may be tolerated during excavation, extensive yielding is generally unacceptable and indicative of a need for redesign. Redesign may require a change in section shape, orientation, or spacing in case of multiple openings.

SHAFTS – FINITE ELEMENT PROCEDURE

A full description of user friendly shaft design is given in the user manual that can be found on the website UT3PC.net along with other documents and software available for download at no cost. Thus, for brevity, only two examples are presented here.

Example 1 – Homestake Mine

This example relates to the Ross Shaft at the former Homestake Mine which is now the Sanford Underground Research Facility (SURF) in Lead, SD. The shaft is a rectangular 15 x 21 ft (3.3 x 6.6 m) section and has recently been rehabilitated from surface to the 4800 Level where a large cavern is being excavated for state of the art neutrino detection. The mine has an admirable history of cooperation with physicists in the detection and study of neutrinos. Rock mechanics study at the mine began in the 1980's (Pariseau 1985) and continued until mine closure in 2002. Rock mechanics studies resumed when the mine was reopened in 2009 with the intent to establish a deep underground research facility.

Step 1. Preparation of a materials property file (stratigraphic column). Rock properties for this example are given in Table 1. These laboratory rock properties values were scaled as a consequence of calibrating finite element models to match extensometer readings of displacement in the mine. The scale factors for elastic moduli and strengths were 0.25 and 0.5, respectively. These two factors are related by guidance from a simple energy relationship (USBM 1995a, 1995b, 1996a).

Table 1. Laboratory Rock Properties for Example 1*

FORMATION PROPERTY	Poorman	Homestake	Ellison
Young's Moduli (GPa)			
Ea	93.1	88.3	89.6
Eb	94.5	62.1	75.8
Ec	49.6	64.2	63.4
Shear Moduli (GPa)			
Ga	26.9	26.9	29.0
Gb	38.6	29.7	35.1
Gc	26.2	33.1	35.7
Poisson's Ratios			
Vab	0.23	0.14	0.20
Vbc	0.22	0.19	0.15
Vca	0.15	0.18	0.17
Compressive Strength (MPa)			
Ca	94.0	138.9	78.2
Cb	84.6	91.5	56.2
Cc	69.0	79.6	78.7
Tensile Strength (MPa)			
Ta	20.6	9.5	16.2

FORMATION PROPERTY	Poorman	Homestake	Ellison
Tb	13.2	13.2	11.4
Tc	5.7	7.9	4.1
Shear Strength (MPa)			
Ra	10.3	14.1	7.9
Rb	8.8	14.5	8.6
Rc	19.3	17.0	14.6

*a=down dip, b=parallel to foliation strike, c=normal to foliation

The material properties file is given in Figure 1. The repetition of the Poorman Formation is a consequence of overturned folds. An unconformity exists above the Ellison Formation, but this feature is of no consequence for the example at hand. Indeed, there is more interesting geology at the mine including rhyolite dikes, but again, of no consequence in this example. The data in Table 1 and Figure 1 reflect an orthotropic anisotropy with axes down dip, on strike, and normal to the foliation. The dip direction is at 55 deg to the y-axis of the finite element mesh (a pseudo-north in this example). Mine north is at 35 deg counter-clockwise to the y-axis of the finite element mesh. The finite element axes are coincident with the shaft axes with the small dimension in the *x*-direction and the long dimension in the *y*-direction. The vertical direction coincides with the *z*-axis. Rotation of material properties from the given material axes (*abc*) is accomplished automatically in accordance with the angles given in the material properties file. In this regard, the first number in the last line of each material is the dip direction (0-360 deg); the second number is the dip (0-90 deg). The third and fourth numbers are depth and thickness, respectively.

```
NLYRS = 3
NSEAM = 2
 (1) Poorman
 13.5e+06 13.7e+06 7.20e+06    0.23    0.22    0.15
  3.8e+06  5.6e+06  3.94e+06     0.0     0.0     0.0
    13630    12270     10000    2990    1910     820
     1500     1520      2800
       55       60      2900     560
 (2) Homestake
 12.8e+06  9.0e+06  9.3e+06    0.14    0.19    0.18
  4.8e+06  4.3e+06  3.9e+06     0.0     0.0     0.0
    20150    13270    11547    1378    1920    1139
     2025     2100     2470
     55.0     60.0   3460.0    80.0
 (3) Poorman
 13.5e+06 13.7e+06 7.20e+06    0.23    0.22    0.15
  3.8e+06  5.6e+06  3.94e+06     0.0     0.0     0.0
    13630    12270     10000    2990    1910     820
     1500     1520      2800
     55.0     60.0    3540.0   560.0
```

```
NLYRS = 3:  Number of layers in the stratigraphic column.
NSEAM = 2:      Layer number of the seam of interest.
 (1) Poorman:          Layer number and formation name.
  E1     E2     E3     v12    v23    v31: Young's moduli,
Poisson's ratios
 G12   G23   G31    γ1     γ2     γ3:  Shear moduli and unit
weight components
 C1    C2    C3    T1    T2    T3: unconfined compressive
and tensile strengths
 R1    R2    R3              : shear strengths
  α   β   dpth   thick   : dip direction, dip, depth, thickness
```

Figure 1. Material properties file for Example 1 and Key. Units are psi for moduli and strengths in accordance with program input requirements. Depth and thickness are in feet.

Step 2. Mesh Generation. Mesh generation input is given in an InData file that is developed during mesh generation: Thus,

```
Input Data
 SHAFT NPROB 6
 Shaft Shape = Rectangle
 Shaft System = Single Opening
 Shaft Width =      15.0
 Width/Height Ratio =       0.7
 Opening Height=      21.0
 Section Depth Seam Center (ft)   =    3500.0
 Additional Sxx,Syy,Szz,Tyz,Tzx,Txy, tension +=
   -3349.0   -2704.0   -4167.0       0.0       0.0    -886.0
 Shaft Stress Sxx,Syy,Szz,Tyz,Tzx,Txy, tension +=
   -3349.0   -2704.0   -4167.0       0.0       0.0    -886.0
```

The preexcavation stresses are developed during mesh generation. If unit weights are present in the material properties file, then gravity stresses are computed. Additional stresses may then be added to any gravitational stress to obtain the pre-excavation stresses.

The premining stresses in this example were obtained from formulas developed for the Homestake Mine (USBM 1996a) in the mine coordinate system. Rotation to finite element coordinates results in the stresses shown in the InData file above. This rotation of stress must be done offline before mesh generation. The given values take into account stress caused by gravity, so no specific weights are present in the material properties file, Figure 1.

A mesh plot is shown in Figure 2 in plan view. The mesh is actually a slab and has a thickness into the page. There are 73,728 nodes and 36,384 three-dimensional elements in the slab.

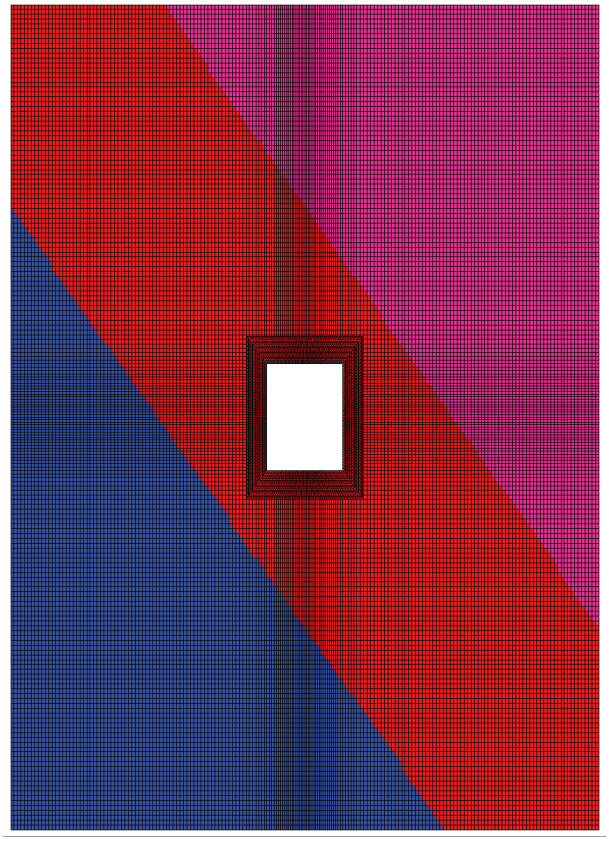

Figure 2. A mesh plot for an Example 1 of a deep, rectangular mine shaft. Magenta=Poorman Formation. Dark Red=Homestake Formation. Blue=Poorman Formation (again). The short dimension of the shaft is 15 ft (4.5 m); the long dimension of the shaft is 21 ft (3.3 m) and bears 35 degrees clockwise from mine north. The mesh is approximately 112 x 158 ft (34 x 48 m).

Step 3 Finite element method (FEM) Execution and Results. The runtime of this model is 7 minutes. Figure 3 shows results in the form of the consequent distribution of element safety factors. The skewed distribution is a consequence of the premining stress state. Not too surprisingly, the opposite corners at the shaft wall have the highest and lowest local safety factors, a result that is consistent with detailed studies (Brady et al. 2001). Run time for the analysis is approximately 11.5 minutes.

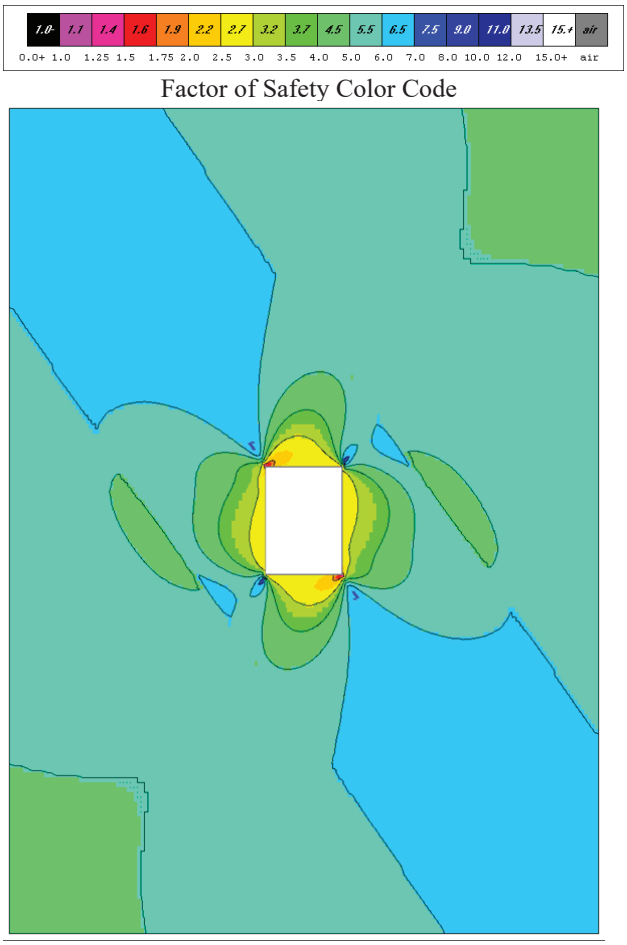

Figure 3. Element safety factors (laboratory rock properties and a thin Homestake Formation). Most of the shaft wall is yellow and has a safety factor of 2.7.

A more realistic analysis considers rock properties scaled to match mine measurements. The element safety factor distribution at shaft level is shown in Figure 4. No element failures occurred, although the highly stressed corner elements have safety factors of 1.4 as seen in the color scale.

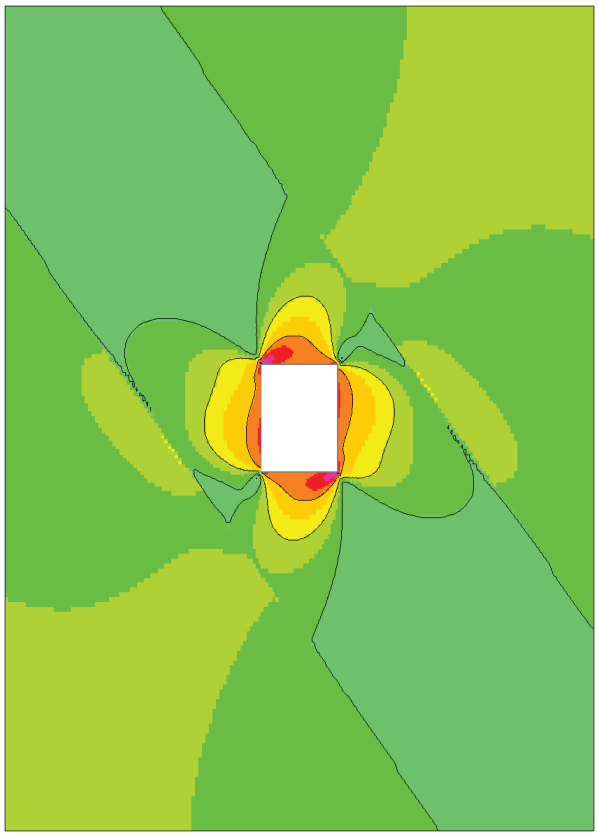

Figure 4. Element safety factors (scaled elastic moduli and strengths at 0.25 and 0.50, respectively). Most of the shaft wall is orange and has a safety factor of 1.9.

In fact, the Ross Shaft has remained safe until long-term creep closure had exhausted shaft guide adjustment with a consequent sticking of the cage and development of slack rope. This dangerous development was initially attributed to shaft pillar mining and the first shaft pillar blast round. However, instrumentation about the shaft indicated no sudden closure with the first round. After considerable discussion with mine management, miners, state and federal health and safety officials, and presentation of shaft monitoring data in conjunction with numerical modeling, a decision was made to excavate behind the shaft framing and to regain proper guide clearance. Monitoring with multi-point extensometers in the Ross Shaft pillar continues to this day, and the shaft remains safe.

Example 2 – Lucky Friday Mine

This example is motivated by mine shafts in the famous Coeur d'Alene Mining District of Northern Idaho where shafts were rectangular at the beginning of district development. At the Lucky Friday Mine, the shape of the Silver Shaft was changed to circular and then to elliptical as ore was pursued to depth.

Step 1. Preparation of a materials property file (stratigraphic column). Material properties for this example are estimated from several sources as indicated in Table 2. Data in the table reflect transversely isotropic rock. The geological setting is one of Precambrian meta-sediments: sericitic quartzites, argillitic quartzites, and vitreous quartzites.

Table 2. Estimated Rock Properties for Example 3*†

FORMATION PROPERTY	Vitreous Quartzite	Sericitic Quartzite	Argillitic Quartzite
Young's Moduli (GPa/Mpsi)			
Ea	42.1/6.1	37.9/5.5	29.0/4.2
Eb	42.1/6.1	37.9/5.5	29.0/4.2
Ec	42.1/6.1	27.6/4.0	12.4/1.8.
Shear Moduli (GPa/Mpsi)			
Ga	16.5/2.4	13.1/1.9	7.61/1.1
Gb	16.5/2.4	13.1/1.9	7.61/1.1/
Gc	16.5/2.4	15.9/2.3	12.4/1.8
Poisson's Ratios			
Vab	0.26	0.21	0.18
Vbc	0.26	0.20	0.11
Vca	0.26	0.20	0.11
Compressive Strength (MPa/psi)			
Ca	169 /24,500	120 /17,470	59/8,500
Cb	169/ 24,500	120/ 17,470	59/8,500
Cc	169/ 24,500	180 /26,040	84/12,230
Tensile Strength (MPa/psi)			
Ta	19.3/ 2,800	16.1/ 2,330	19.2/2,790
Tb	19.3/ 2,800	16.1/ 2,330	19.2/2,790
Tc	15.2/ 2,200	10.6/ 1,530	7.4/1,080
Shear Strength (MPa/psi)			
Ra	29.2/ 4,240	25.4 /3,680	19.4/ 2,820
Rb	29.2 /4,240	25.4/ 3,680	19.4/ 2,820
Rc	33.0/ 4,780	25.1/ 3,640	30.4/ 4,400

*a=down dip (parallel to bedding), b=parallel to bedding on strike, c=normal to bedding

†With guidance from Whyatt (1986); Board and Beus (1989); USBM (1996b); Sturgis et al. (2017).

Step 2. Mesh Generation. Mesh generation input was developed for three shaft shapes, circular, elliptical-1, 6.1x7.0 m (20x23 ft), and elliptical-2, 6.1x7.9 m (20x26 ft). Orientation of foliation (dip direction) is 195 deg for the circular section, measured from the *y*-axis of the finite element model. Dip is 80 deg. Orientation of foliation is 180 deg for the elliptical sections. These angles are shown in the material properties files for circular and elliptical sections. Thus, for a circular section

```
NLYRS = 1
NSEAM = 1
 (1) Argillitic Quartzite
  4.2e+06  4.2e+06  1.8e+06     0.18     0.11     0.11
  1.1e+06  1.1e+06  1.8e+06      0.0      0.0      0.0
   8500.0   8500.0  12230.0   2790.0   2790.0   1080.0
   2820.0   2820.0   4400.0
    195.0     80.0   8500.0    400.0
```

and for elliptical sections

```
NLYRS = 1
NSEAM = 1
 (1) Argillitic Quartzite
  4.2e+06  4.2e+06  1.8e+06     0.18     0.11     0.11
  1.1e+06  1.1e+06  1.8e+06      0.0      0.0      0.0
   8500.0   8500.0  12230.0   2790.0   2790.0   1080.0
   2820.0   2820.0   4400.0
    180.0     80.0   8500.0    400.0
```

The elastic moduli and strengths were reduced from the values in Table 2 by scale factors or 0.25 and 0.50, respectively. Moduli in the finite element analyses were one-fourth of those in the table; strengths were one half of the table values. These were the same scale factors used in the Homestake Mine shaft example to account for "joints" at the mine scale. The model constructed has 36,384 elements and 73,728 nodes.

An InData file example for an elliptical section 20 x 23 ft (6.1x7.0 m) is

```
Input Data
 SHAFT NPROB 6
 Shaft Shape = Ellipse (including circle)
 Shaft System = Single Opening
 Shaft Width =              20.0
 Width/Height Ratio =        0.9
 Opening Height=            23.0
 Section Depth Seam Center (ft)   =    8700.0
 Additional Sxx,Syy,Szz,Tyz,Tzx,Txy, tension +=
  -11407.0  -10549.0   -9640.0      0.0      0.0   1220.0
 Shaft Stress Sxx,Syy,Szz,Tyz,Tzx,Txy, tension +=
  -11407.0  -10549.0   -9640.0      0.0      0.0   1220.0
```

The stress input data are derived from formulas given by Board and Beus (1989) using a depth of 8,700 ft. Rotation of these data to finite element coordinates was necessarily done prior to mesh generation. The first ellipse mesh is shown in Figure 5.

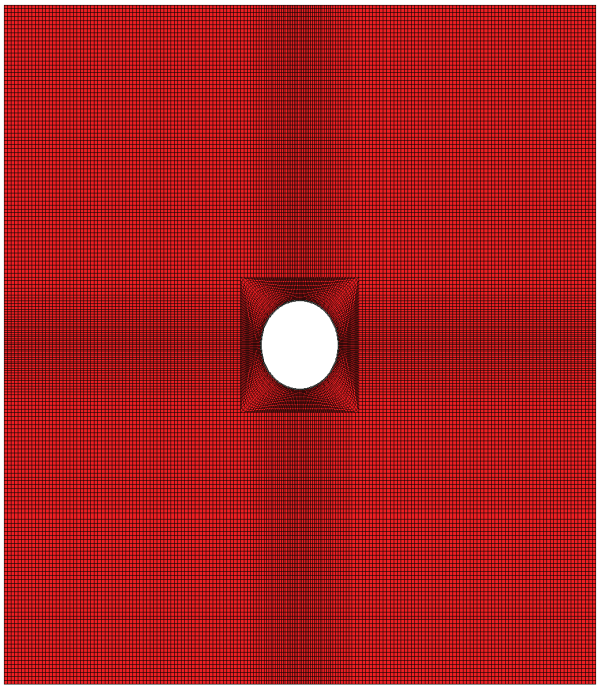

Figure 5. Elliptical shaft section 6.1x7.0 m (20x23 ft).

Step 3. FEM Execution and Results. Model runtime is 10 minutes. Distribution of element safety factors in case of the circular and first elliptical sections are shown in Figure 6.

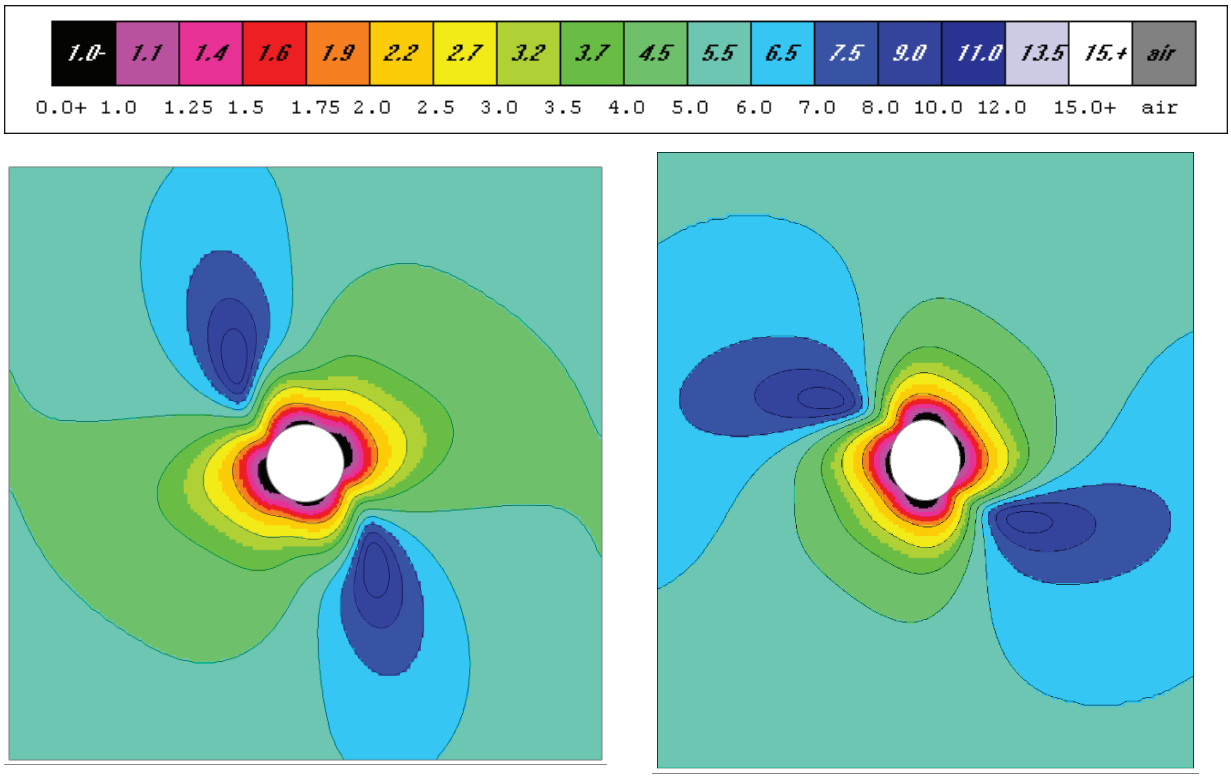

Figure 6. Element safety factor distributions around (A) circular and (B) elliptical shaft sections.

The yielding elements in both sections of Figure 6 are mainly perpendicular to the foliation, although the orientation is different in the two parts of the figure. The number of yielding elements is slightly smaller in the ellipse and somewhat less in a second ellipse of 6.1x7.9 m (20x26 ft), but the differences are small. In this regard, the rule for minimizing stress concentration that guides elliptical sections ("long axis parallel to the major principal stress") for isotropic rock is not applicable in this situation. Additionally, there are orientation differences between principal stress in the plane of the section and the foliation.

In this example, foliation appears to rule as Figure 7 shows. In this figure, the major principal stress is perpendicular to the long axis of the ellipse contrary to the isotropic rule, but the major principal stress is also parallel to the foliation and highest compressive strength direction.

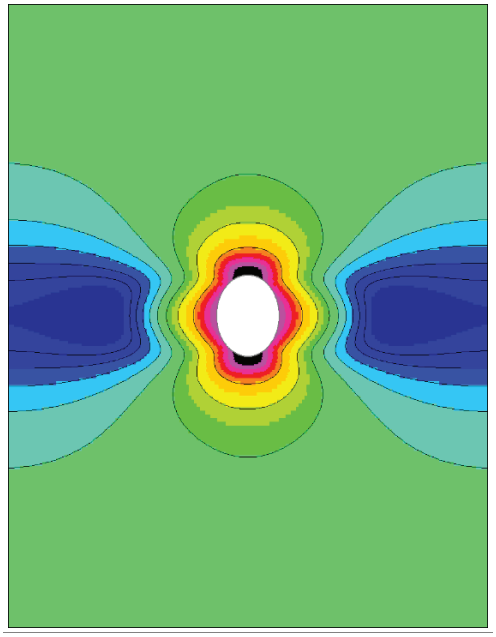

Figure 7. Element safety factor distribution about an ellipse 6.1x7.9 m (20x26 ft) with the major principal stress and foliation aligned with the minor axis of the ellipse.

The actual shape appears more in keeping with breakouts than a true ellipse (Sturgis et al. 2017). A more detailed study would certainly be of interest, but such is beyond the scope of this demonstration. However, these results do indicate fast, easy-to-use software capability for analysis of shaft safety.

TUNNELS – FINITE ELEMENT PROCEDURE

Tunnels here include adits, crosscuts and drifts (in mine-speak) as well as tunnels in the usual meaning of the word. As in analyses of shafts, concern here is with the redistribution of stress induced by excavation and the consequent distribution of tunnel wall safety factors. The safety of tunnel excavations is of most importance, less so than numerical values of stress and strain associated with excavation. Displacements of unlined mine tunnels immediately after excavation are also of less concern, especially when assurance of an elastic response to excavation is obtained. As a reminder, an elastic ideally plastic stress-strain law is used in the three-dimensional finite element analyses presented here. Neither work-hardening nor softening occur beyond the elastic limit; time-dependent behavior is not allowed.

Side-by-side or twin tunnels are of interest. Indeed, multiple tunnels (entries, drifts, crosscuts) may be used in large underground mines to ensure adequate ventilation and haulage capacity. Separation of tunnels in a row by pillars is an important consideration in case of multiple tunnels of the same cross-section.

Tunnel mesh generation allows for single, twin, and rows of tunnels side by side. Circular, rectangular, and elliptical cross-sections are allowed in every case as in the analyses of shafts. Importantly, the frequently used arched back shape is also allowed.

Example 3a – Stillwater Mine

An example of circular tunnels is one motivated by long adits excavated by boring machines at the East Boulder project of the Stillwater Mine in south-central Montana. Adit diameters of 13, 15 and 18 ft were excavated (Luxner et al. 2012)

Step 1. Preparation of a materials property file (stratigraphic column). The material properties file for this example is

```
NLYRS = 1
NSEAM = 1
 (1) Gabbro Reef
 15.8e+06  15.8e+06  15.8e+06      0.25      0.25      0.25
 6.32e+06  6.32e+06  6.32e+06       0.0       0.0       0.0
  28000.0   28000.0   28000.0    1600.0    1600.0    1600.0
   3910.0    3910.0    3910.0
     90.0      90.0     290.0     420.0
```

Step 2. Mesh Generation. Mesh generation input is given in the InData file that is developed during mesh generation. Thus,

```
Input Data
 DRIFT NPROB 7
 Tunnel Shape = Ellipse (including circle)
 Tunnel System = Twin Openings
 Tunnel Width =      15.0
 Width/Height Ratio =       1.0
 Pillar Width =      30.0
 Section Depth Seam Center (ft)   =    2600.0
 Additional Sxx,Syy,Szz,Tyz,Tzx,Txy, tension +=
   -5616.0   -3120.0   -4680.0       0.0       0.0       0.0
 Tunnel Stress Sxx,Syy,Szz,Tyz,Tzx,Txy, tension +=
   -5616.0   -3120.0   -4680.0       0.0       0.0       0.0
```

The premining stresses were estimated from formulas and guidance presented in Langston and Kirsten (2002) and Johnson et al. (2003). Stresses are with respect to compass coordinates that are also mine coordinates in this example. Note: The vertical stress is Syy in tunnel analyses.

A mesh plot is shown in Figure 8 in cross-section. The mesh is actually a slab and has a thickness into the page. There are 15,088 elements and 32,218 nodes in the slab.

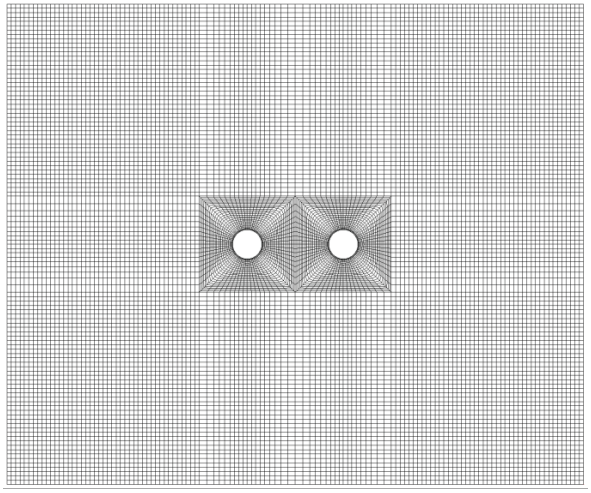

Figure 8. Finite element mesh for twin tunnels (adits) at the Stillwater Mine. Tunnel diameters are 15 ft (4.6 m); pillar width is 30 ft (9.1 m). Depth is 2,600 ft (793m).

Step 3. FEM Execution and Results. Model runtime was 5 minutes. Figure 9 shows results in the form of the distribution of element safety factors. As before, the elastic moduli and strengths at the laboratory scale were reduced using scale factors of 0.25 and 0.5, respectively. The pillar width is evidently adequate to prevent elevated stress arising from tunnel interaction.

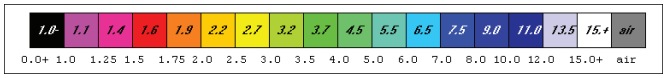

Factor of Safety Color Code

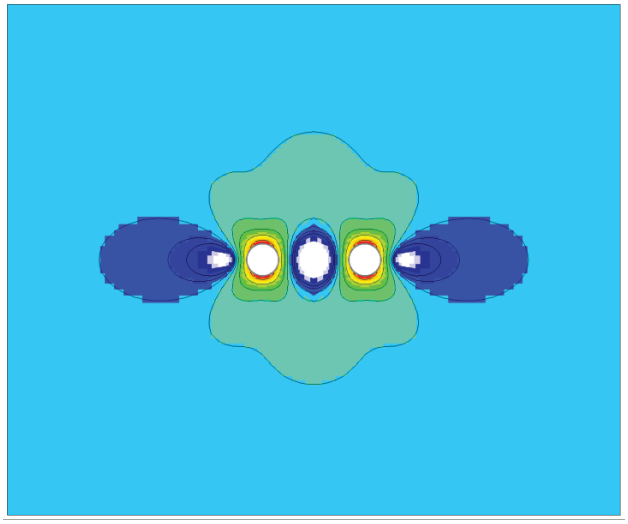

Figure 9. Element safety factors about twin tunnels excavated by a tunnel boring machine at the Stillwater Mine (East Boulder). Safety factors range from 1.6 (orange) to over 15 (white).

As always in these examples, the intent is to demonstrate the capability of user friendly software for fast, reliable analysis of excavation safety using reasonable conditions in situ. A detailed, site-specific engineering design analysis is not the intention here.

Example 3b – Stillwater Mine (With Joints)

A non-representative volume element (NRVE) approach to accommodate joint effects on tunnel safety is needed when the elements are too small to be representative, that is, to include many joints. This situation is almost always the case and is certainly the case in this example of twin adits. Elements at the adit walls are approximately 0.3 ft (0.1 m) on edge; spacing of joints in Set 1 is 3 ft (0.9 m) and in Set 2 spacing is 4.4 ft (1.3 m). Thus, maximum joint spacing is 4.4 ft (1.3 m). A schematic view of the two joint sets is shown in Figure 10. The intersection of joints creates many joint segments that are recognized as distinct joints even within a single finite element.

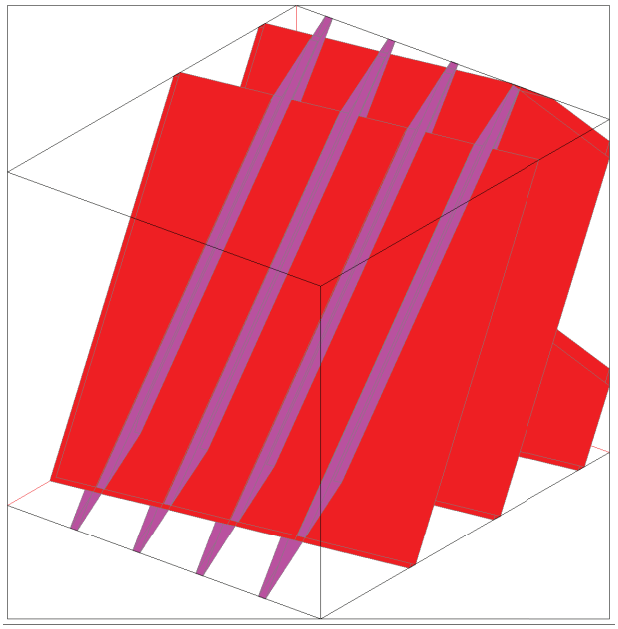

Figure 10. Schematic of two joint sets in Example 3b. Magenta=Set 1, Red=Set2.

The result of a NRVE analysis is the element safety factor distribution shown in Figure 11. Safety factors in the figure are for intact rock present in each element and are relatively high (green=5.0, blue=10).

Factor of Safety Color Code

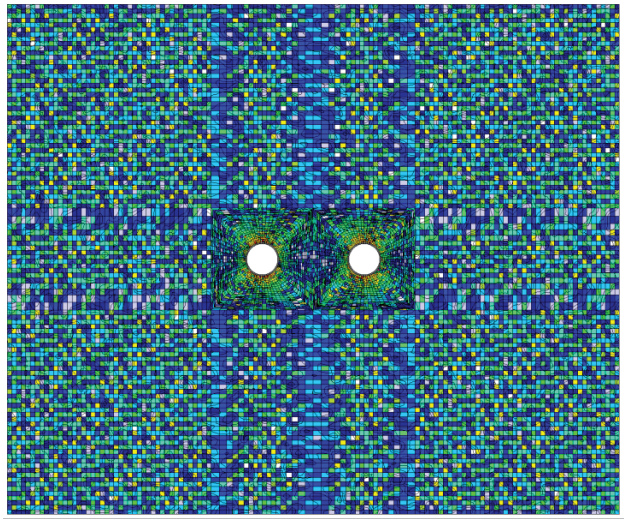
(A) Whole Mesh

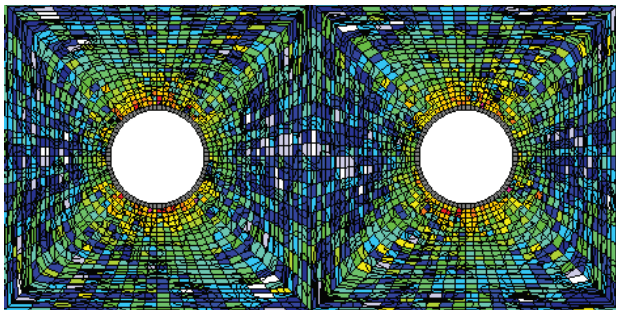

(B) Close Up

Figure 11. Element safety factor distribution relative to intact rock in a twin bore tunnel NRVE analysis of jointed rock.

Details of mesh and intact rock properties are the same as in the previous example where joints are not present. There are 15,808 elements and 20,748 joint segments in the mesh. No element failures occur, but 16,043 joint segments fail. Element safety factors in the figure are based on intact rock strength and average stress in an element. However, the close-up view indicates a number of elements at the tunnel walls with intact rock safety factors less than two. Conventional wall support and reinforcement would certainly be required.

Joint failures are shown in Figure 12. They are widespread as seen in the figure with more joints in Set 2 (yellow) failing than in Set 1 (red).

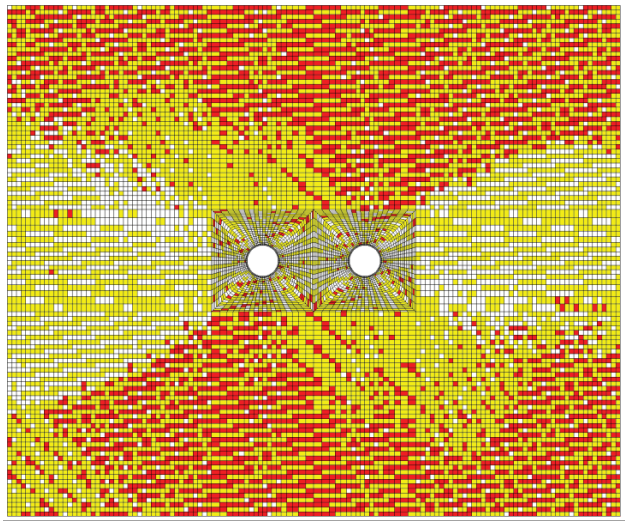

(A) Whole Mesh

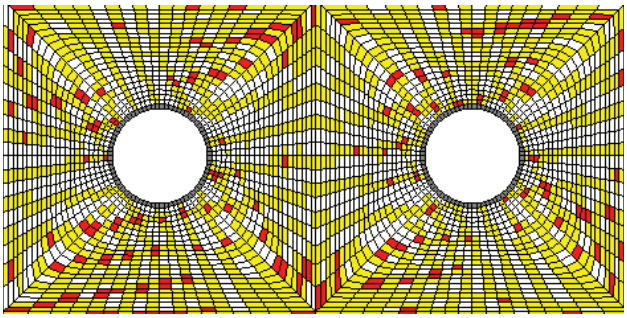

(B) Close Up

Figure 12. Joint failures: RED=joints in joint set 1 failures. YELLOW=joints in joint set 2 failures, WHITE=no joint failures. Tunnels are 15 ft (4.6 m) in diameter and are separated by a 30-ft (9.1-m) pillar.

Although the safety factor distribution relative to intact rock in Figure 11 indicates safety, whether the joint failures shown in Figure 12 indicate a threat to safety is an open question. Does joint failure in an element indicate whole element failure? If so, then almost all elements in the mesh fail, an unlikely physical result, especially in elements far from the tunnels. In this regard, software from one well-known consultancy does consider an element or cell to fail if any joint in the element fails. The question is certainly worthy of study because of the practical importance of the issue, but one that is beyond the scope of this work.

To be sure, generation of jointing and embedment into the finite element mesh is not currently available in the FEM software made freely available on UT3PC.net at this juncture, but it is an objective for future technology transfer.

Example 4 – Homestake Mine

Examples of a single, arched-back drift and an arched-back crosscut at the former Homestake Mine in the Northern Black Hills of South Dakota are compared in this composite example. The geology of the mine is characterized by three major formations, the Poorman, Homestake, and Ellison, consisting of Precambrian meta-sediments (phyllite, schist, and gneiss).

Step 1. Preparation of a materials property file (stratigraphic column). Rock properties for this example are given in Table 1. These laboratory rock properties values were scaled as a consequence of calibrating finite element models to match extensometer readings of displacement in the mine. The scale factors for elastic moduli and strengths were 0.25 and 0.5, respectively.These two factors are related by guidance from a simple energy relationship (USBM 1995a, 1995b, 1996a).

The material properties file for the drift is given in Figure 13. The data in Table 1 and Figure 13 reflect an orthotropic anisotropy with axes down dip, on strike, and normal to the foliation. The dip direction is at 90 deg to the y-axis of the finite element mesh (a pseudo-north in this example), that is, due east for the drift and parallel to north in the crosscut case.

```
NLYRS = 3
NSEAM = 3
 (1) Ellison
 13.0e+06  11.0e+06  9.19e+06      0.20      0.15      0.17
  4.2e+06  5.09e+06  5.18e+06       0.0       0.0       0.0
  11339.0    8149.0   11411.0    2349.0    1653.0     594.0
   1145.0    1247.0    2117.0
     90.0      70.0    3680.0     700.0
 (2) Homestake
 12.8e+06   9.0e+06   9.3e+06      0.14      0.19      0.18
  4.8e+06   4.3e+06   3.9e+06       0.0       0.0       0.0
  20150.0   13270.0   11547.0    1378.0    1920.0    1139.0
   2025.0    2100.0    2470.0
     90.0      70.0    4380.0     120.0
 (3) Poorman
 13.5e+06  13.7e+06  7.20e+06      0.23      0.22      0.15
  3.8e+06   5.6e+06  3.94e+06       0.0       0.0       0.0
  13630.0   12270.0   10000.0    2990.0    1910.0     820.0
   1500.0    1520.0    2800.0
     90.0      70.0    4500.0     700.0
```

Figure 13. Material properties file for Example 4. In Example 4, the dip direction is due north (0 deg).

Step 2. Mesh Generation. Mesh generation input is given in the InData file that is developed during mesh generation for the drift. Thus for the drift:

```
Input Data
 DRIFT NPROB 7
 Tunnel Shape = Arched Rectangle
 Tunnel System = Single Opening
 Tunnel Width =       8.0
 Width/Height Ratio =       1.0
 Tunnel Height=       8.0
 Section Depth Seam Center (ft)   =    4850.0
 Additional Sxx,Syy,Szz,Tyz,Tzx,Txy, tension +=
   -4648.0   -2788.0   -6062.0       0.0       0.0       0.0
 Tunnel Stress Sxx,Syy,Szz,Tyz,Tzx,Txy, tension +=
  -4648.0   -6062.0   -2788.0       0.0       0.0       0.0
```

and for the crosscut:

```
Input Data
 CROSSCUT NPROB 7
 Tunnel Shape = Arched Rectangle
 Tunnel System = Single Opening
 Tunnel Width =       8.0
 Width/Height Ratio =       1.0
 Tunnel Height=       8.0
 Section Depth Seam Center (ft)   =    4850.0
 Additional Sxx,Syy,Szz,Tyz,Tzx,Txy, tension +=
   -2788.0   -6062.0   -4648.0       0.0       0.0       0.0
 Tunnel Stress Sxx,Syy,Szz,Tyz,Tzx,Txy, tension +=
   -2788.0   -6062.0   -4648.0       0.0       0.0       0.0
```

Note the vertical stress is the same (Syy), but the horizontal stresses are reversed in keeping with the change in drift direction along strike to crosscut direction perpendicular to the strike direction.

The premining stresses were obtained from formulas developed for the Homestake Mine that are with respect to mine coordinates. The given values take into account stress caused by gravity, so no specific weights are present in the material properties file, Figure 13.

A mesh plot is shown in Figure 14in vertical section. The mesh is actually a slab and has a thickness into the page. There are 73,728 nodes and 36,384 three-dimensional elements in the slab.

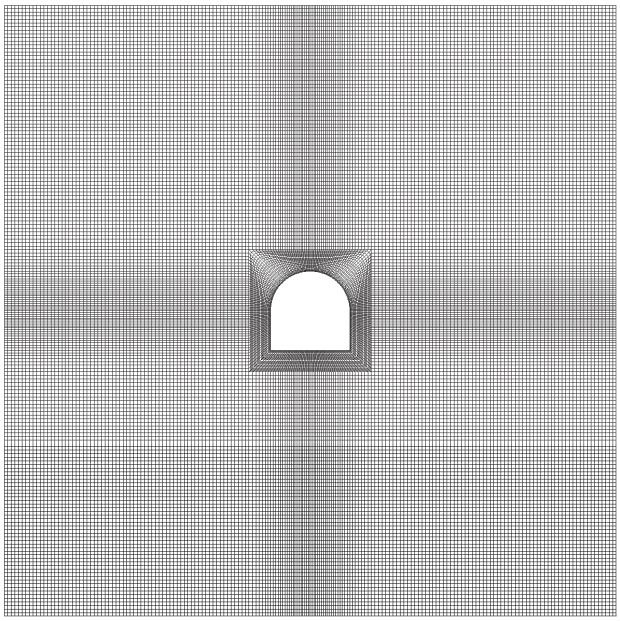

Figure 14. Example 2a,b mesh of an 8 x 8 ft (2.4 x 2.4 m) arched-back drift and crosscut.

Step 3. FEM Execution and Results. Figure 15 shows results in the form of the consequent distribution of element safety factors. The drift plot shows red farther into the ribs of the drift than the crosscut. In fact,

experience shows drifts along the “grain” are more likely to require support than crosscuts across the grain.

In Figure 15, ribs are in yellow (2.5) in the drift where some floor and back failure is indicated in black (1.0). Crosscut back and floor are in red (1.5). Overall the crosscut appears less threatened than the drift. This result is in keeping with visual observations at the mine.

CONCLUSION

Shafts, winzes and raises, tunnels, adits, drifts and crosscuts are lifelines to the underground and must remain safe and secure for the life of a mine. While support and reinforcement aid in securing the immediate walls of a shaft or tunnel, strength of the rock walls in situ is relied upon to provide the natural support needed for immediate safety and long-term stability. In this regard, a useful engineering index to safety is a factor of safety (fs) defined as a ratio of “strength” to “stress,” that is, $fs = strength/stress$ where suitable three-dimensional measures of strength and stress are invoked. If fs>1, then the stress state is in the elastic domain. If fs=1, then the limit to elasticity is reached followed by yielding with continued loading.

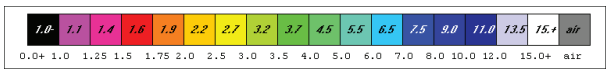

Factor of Safety Color Code

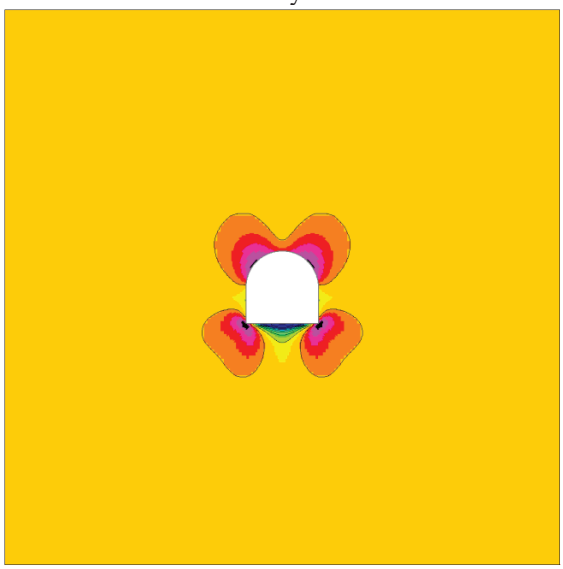

(a) drift

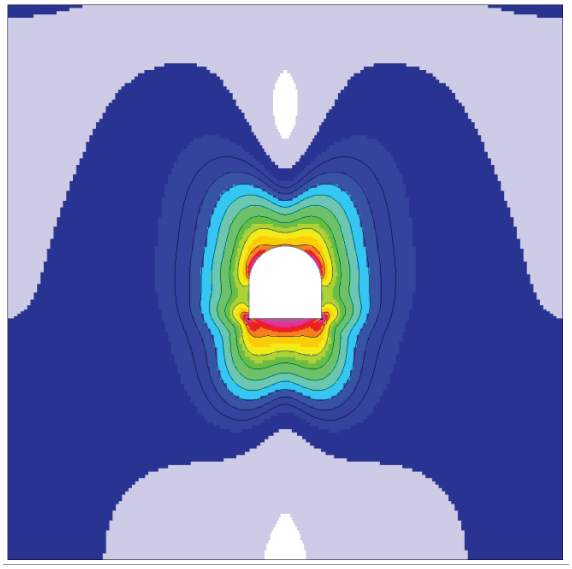

(b) crosscut

Figure 15. Element safety factors about an 8x8 ft (2.4 x 2.4 m) arched back drift (a) and crosscut (b).

Distributions of element safety factors that result from an analysis of stress about a proposed shaft or tunnel layout provide useful guidance to design suitability. There is no sharp divide between suitable designs, marginal designs, and designs that pose undue risk to safety. As always, engineering design requires judgment based on experience as well as based on quantitative analysis founded on first principles such as physical laws, kinematics, and material laws.

User friendly software enables quantitative design in three easy steps: (1) preparation of a rock properties file, (2) mesh generation, and (3) program execution with post-execution plotting of element safety factor distribution. The software and documentation, including an extensive User Manual with numerous explanations, are available at no charge on the website UT3PC.net. The goal is to advance the technology of mine design for the improvement of mine health and safety. One need not be a career numerical modeling expert to benefit from the user friendly software on this website. However, familiarity with the concepts of stress, strain, Hooke’s law, and rock strength that are discussed in mechanics of materials courses at the undergraduate level is expected

ACKNOWLEDGEMENTS

The study of shafts and tunnels was funded in part by the Center for Disease Control and Prevention, National Institute for Occupational Safety and Health (CDC/NIOSH) under contract 75D30120P09279 which

was monitored at the Spokane Mining Research Division (SMRD).

DISCLAIMER

The findings and conclusions in this report are those of the author(s) and do not necessarily represent the official position of the National Institute for Occupational Safety and Health, Centers for Disease Control and Prevention. Mention of any company or product does not constitute endorsement by NIOSH.

REFERENCES

Amadei, B., and Goodman, R. E. 1981. Formulation of complete plane-strain problems for regularly jointed rocks. In *Proceedings of the 22nd U.S. Symposium on Rock Mechancis: Rock Mechanics from Research to Application*. Einstein, H. H., and Scandariato, D. P. eds. (Cambridge, MA: June 29–July 2, 1981) Cambridge, MA: MIT, pp. 265–271.

Beran, M. J. 1968. *Statistical continuum theories*. 1st edn (New York: Interscience Publishers), 424 pp.

Board, M. P., and Beus, M. J. 1989. *In-situ measurements and preliminary design analysis for deep mine shafts in highly stress rock*. By Board MP, Beus MJ. Report of Investigations 9231. Pittsburgh, PA: U.S. Department of the Interior, Bureau of Mines (USBM), 53 pp.

Brady, T. M., Johnson, J. C., Laurenti, M. A., Pariseau, W. G., and Stahl, M. 2001. Mining the remaining portion of the Ross Shaft pillar. In *Rock Mechanics in the National Interest: Proceedings of the 38th U.S. Rock Mechanics Symposium*. Elsworth, D.,Tinucci, J. P., and Heasley, K. A. eds. 1, (Washington, D.C.: June 7–10, 2001) Lisse, Netherlands: Balkema, A. A., pp. 395–399.

Duncan, J. M., and Goodman, R. E. 1968. *Finite element analysis of slopes in jointed rock*. Report No. TE-68-1. Vicksburg, MS: U.S. Army Engineer Waterways Experiment Station, Corp of Engineers, 272 pp.

Gerrard, C. M. 1982. Elastic models of rock masses having one, two and three sets of joints. *Int. J. Rock Mech. Min. Sci. & Geomech. Abstr.,* 19(1): 15–23, https://doi.org/10.1016/0148-9062(82)90706-9.

Hadamard, J. S. 1903. *Lecon sur la propagation des ondes et les equations de l'hydrodynamique* (Paris: Herman [Reprint Chelsea Publishing Company, New York, 1949, 372 pp.]).

Hashin, Z., and Shtrikman, S. 1963. A variational approach to the theory of the elastic behaviour of multiphase materials. *J. Mech. Phys. Solids,* 11(2): 127–140, https://doi.org/10.1016/0022-5096(63)90060-7.

Hill, R. 1967. The essential structure of constitutive laws for metal composites and polycrystals. *J. Mech. Phys. Solids,* 15(2): 79–95, https://doi.org/10.1016/0022-5096(67)90018-X.

Hudson, J. A. 1980. *The excitation and propagation of elastic waves* (Cambridge, U.K.: Cambridge University Press), 226 pp.

Huet, C. 1984. On the definition and experimental determination of effective constitutive equations for assimillating heterogeneous materials. *Mechanics Research Communications,* 11(3): 195–200.

Johnson, J., Brady, T., MacLaughlin, M., Langston, R., and Kirsten, H. 2003. In situ stress measurements at the Stillwater Mine, Nye, Montana. In *Proceedings, Soil and Rock America 2003: 12th Panamerican Conference on Soil Mechanics and Geotechnical Engineering and 39th U.S. Rock Mechanics Symposium*. Culligan, P. J.,Einstein, H. H., and Whittle, A. J. eds. 1, (Cambridge, Massachusetts: June 22–26, 2003) Essen, Germany: Verlag Glückauf, Gmbh, pp. 337–344.

Langston, R., and Kirsten, H. 2002. *Ground Control Manual*. Nye, MT: Stillwater Mining Company.

Luxner, T., Deen, J., and Koski, M. 2012. Use Of Tunnel Boring Machines At The Stillwater Mining Company's Underground PGM Mines. *Mining Eng.,* 64(12): 50–57.

Morland, L. W. 1974. Continuum model of regularly jointed mediums. *J. Geophys. Res.,* 79: 357–362.

Pariseau, W. G. 1985. *Research study on pillar design for Vertical Crater Retreat (VCR) mining*. U.S. Bureau of Mines Final Report. Contract J021503. Salt Lake City, UT: University of Utah, 234 pp.

Pariseau, W. G. 1988. On the concept of rock mass plasticity. In *Key Questions in Rock Mechanics: Proceedings of the 29th U.S. Symposium*. Cundall, P. A.,Sterling, R. L., and Starfield, A. M. eds. (Minneapolis: June 13–15, 1988) Rotterdam: Balkema, A. A., pp. 291–302.

Pariseau, W. G. 1995. Non-representative volume element modeling of equivalent jointed rock mass properties. In *Proceedings of the Second International Conference on the Mechanics of Jointed and Faulted Rock—MJFR-2*. Rosmanith, H.-P. ed., (Vienna, Austria: April 10–14, 1995) Rotterdam: Balkema, A. A., pp. 563–568.

Pariseau, W. G., Larson, M. K., Lawson, H. E., and Tesarik, D. R. 2017. User-friendly finite element

design of main entries, barrier pillars, and bleeder entires. In *Proceedings of the 36th International Conference on Ground Control in Mining.* Mishra, B.*, et al.* eds. (Morgantown, WV: July 25–27, 2017) Englewood, CO: Society for Mining, Metallurgy & Exploration (SME), 12 pp.

Pariseau, W. G., Larson, M. K., and Nelson, M. G. 2020. User-friendly finite element analysis of five mine design problems. In *Preprints, SME Annual Meeting & Exhibit.* (Phoenix, AZ: February 23–26, 2020) Englewood, CO: Society for Mining, Metallurgy, and Exploration, Inc., 4 pp.

Pariseau, W. G., and Moon, H. 1988. Elastic moduli of well-jointed rock masses. In *Proceedings of the Sixth International Conference on Numerical Methods in Geomechanics*. Swoboda, G. ed., (Innsbruck, Austria: April 11–15, 1988) Rotterdam: Balkema, A. A., pp. 815–822.

Pinto da Cunha, A. 1990. Scale Effects in Rock Mechanics. In *Scale Effects in Rock Masses: Proceedings of the First International Workshop on Scale Effects in Rock Masses*. Pinto da Cunha, A. ed., (Loen, Norway: June 7–8, 1990) Rotterdam: Balkema, A. A., p. 27.

Salamon, M. D. G. 1968. Elastic moduli of a stratified rock mass. *Int. J. Rock Mech. Min. Sci. & Geomech. Abstr.,* 5(6): 519–527, https://doi.org/10.1016/0148-9062(68)90039-9.

Shi, G.-H., Goodman, R. E., and Tinucci, J. P. 1985. Application of block theory to simulated joint trace maps. In *Proceedings of the International Symposium on Fundamentals of Rock Joings*. Stephansson, O. ed., (Luleå, Sweden: September 15–20, 1985) Björkliden, Sweden: Centek Publishers,, pp. 367–383.

Sturgis, G. A., Berberick, D., Board, M. P., Strickland, W. H., and Swanson, M. T. 2017. Elliptical shaft excavations and furnishing in response to depth induced ground pressure. In *Deep Mining 2017: Proceedings of the Eighth International Conference on Deep and High Stress Mining*. Wesseloo, J. ed., (Perth, Australia: March 28–30, 2017) Perth, Australia: Australian Centre for Geomechanics, pp. 883–898.

Teply, J. L., and Dvorak, G. J. 1987. Dual estimates of overall instantaneous properties of elastic-plastic composites. In *Continuum Models of Discrete Systems: Proceedings of the Fifth International Symposium*. Spencer, A. J. M. ed., (Nottingham: July 14–20, 1985) CRC Press, pp. 205–216.

USBM 1995a. *Rock mechanics study of shaft stability and pillar mining, Homestake Mine, Lead, SD (in three parts). 1. Premining geomechanics modeling using UTAH2*. By Pariseau WG, Johnson JC, McDonald MM, Poad ME. Report of Investigations 9531. Pittsburgh, PA: U.S. Department of the Interior, Bureau of Mines (USBM), 21 pp.

USBM 1995b. *Rock mechanics study of shaft stability and pillar mining, Homestake Mine, Lead, SD (in three parts). 2. Mine measurements and confirmation of premining results*. By Pariseau WG, Johnson JC, McDonald MM, Poad ME. Report of Investigations 9576. Pittsburgh, PA: U.S. Department of the Interior, Bureau of Mines (USBM), 22 pp.

USBM 1996a. *Rock mechanics study of shaft stability and pillar mining, Homestake Mine, Lead, SD (in three parts). 3. Geomechanical monitoring and modeling using UTAH3*. By Pariseau WG, Johnson JC, McDonald MM, and Poad ME. Report of Investigations 9618. Pittsburgh, PA: U.S. Department of the Interior, Bureau of Mines (USBM), 36 pp.

USBM 1996b. *Strength and deformation properties of belt strata, Coeur d'Alene Mining District, ID*. By Whyatt JK, White BG Johnson JC. Report of Investigations 9619. Pittsburgh, PA: U.S. Department of the Interior, Bureau of Mines (USBM), 65 pp.

Whyatt, J. K. 1986. *Geomechanics of the Caladay Shaft*. (M.S. thesis), University of Idaho. 195 pp.

END